



ORIGINAL RESEARCH ARTICLE

Experimental Investigation of Corten Steel Using Cold Metal Transfer Welding

Sreejith S. Nair, I. Rajendran, and T. Ramkumar

Submitted: 23 August 2023 / Revised: 7 October 2023 / Accepted: 20 October 2023 / Published online: 14 November 2023

High strength low alloy steels which are having excellent corrosion-resistant properties are called corten steels. In the present investigation, 3 mm thick ASTM A242 Corten steel sheets were welded together using the cold metal transfer (CMT) method based on two welding controllable parameters like welding current and welding speed. The controllable input parameters like welding current and welding speed have been altered to produce joints that have no flaws and a complete depth of weld penetration. The evaluation of the microstructure and weld geometry was performed for the cold metal transfer welded ASTM A242 sheets using ER70S6 filler wire. The experimental design of welding parameters was developed using an orthogonal array of full factorial design. The dominance of acicular ferrite microstructure is visible in the fusion zone. Results from Energy Dispersive x-Ray Analysis (EDAX) show that manganese content is higher and nickel concentration is lower in the weld fusion region. The fusion zone of the CMT welded specimen has the greatest hardness, which was measured at 270.2 HV. Due to the formation of acicular and bainite microstructure in the welding seam, the tensile properties at room temperature (RT) were found to be 589.79 and 405.63 MPa, accordingly. Bend tests additionally confirmed the satisfactory ductility of the welded joint.

Keywords cold metal transfer welding, corten steel, mechanical properties, microstructure

1. Introduction

Fabrication industry mainly focuses on introducing materials having the combined qualities of mechanical strength and corrosion resistance behavior for getting better performance. Corten is a trade name for weathering steels that were manufactured especially for ensuring better tensile strength along with excellent corrosion resistance. This will be a milestone for the metal fabrication industry sector which is mainly focusing on minimizing lead time, long-term cost savings, and performance. Corten steel is notable for its exceptional strength with low alloying element content, in addition to its excellent corrosion resistance to elements from the environment and high strength-to-weight ratio among carbon steels (Ref 1, 2). The corten steel has an excellent ability to control oxygen reaction with the metal surface to prevent rusting and the delamination of the rust layer over time (Ref 3). The presence of alloying elements like chromium, copper, and nickel, resulting in superior resistance to corrosion, differentiates corten steel from common structural steel in the

aspect of metallurgical characteristics. Corten steel contains acicular ferrite, which improves corrosion resistance by producing an adhering protective coating on the surface, shielding it from corrosive conditions (Ref 4). Due to the presence of protective coating using alloying elements such as Mo, Cr, Cu, Ni, and Si, the weathering steels can be suggested for exploring applications in outdoor environments (Ref 5). In 2004 Fronius of Austria developed an advanced version of metal inert gas (MIG) welding (Ref 6). The CMT process is a modern welding technique that offers advantages such as reduced heat input, minimized distortion, and enhanced control over the welding parameters (Ref 7). The mechanical and microstructural properties of the weld such as weld strength, micro hardness, corrosion behavior, surface morphology, ductility, and fracture mechanism, might be used to evaluate the efficiency of CMT welded joints. Researchers that are looking into the cladding process are becoming progressively attracted in CMT as an advanced welding technique (Ref 8). The advancements in computer technology in the 1990 s have allowed for the design of unlimited waveforms to improve the timing of arcing and metal deposition, giving welders more options in determining welding parameters (Ref 9).

The choice of welding material has a significant influence on the microstructure and properties of welded joints in bridge weathering steel and variations in microstructure due to different welding materials can lead to differences in strength and toughness levels. The welding of weathering steel may result in a more gradual transition from the heat-affected zone (HAZ) to the base material zone, minimizing the risk of stress concentrations and brittleness (Ref 10). The choice of welding material can also impact the susceptibility to cracking, including hydrogen-induced cracking and cold cracking. Proper selection of welding consumables and welding procedures can mitigate these risks. ASTM A242 Corten steel joining using the

Sreejith S. Nair and T. Ramkumar, Department of Mechanical Engineering, Dr. Mahalingam College of Engineering & Technology, Pollachi, Coimbatore Dist, Tamilnadu, India; and I. Rajendran, Department of Mechanical Engineering, Paavai Engineering College, Pachal, Namakkal Dist, Tamilnadu, India. Contact e-mails: sreeju2786@gmail.com, srjth.nair@gmail.com, irus_rajendran@yahoo.co.in, and ramkimech89@gmail.com.

CMT welding process requires specific considerations due to the material's unique characteristics and the process itself. From the literature survey it is clearly understood that only a few investigations were made on the mechanical characteristics and microstructure studies of Corten Grade steels and no specific comprehensive investigation on welding of ASTM A242 steel has been done using advanced welding process like cold metal transfer welding. The available literature lacks an in-depth analysis that connects the controllable welding parameters, mechanical and microstructural properties of ASTM A242 steel using advanced joining techniques such as cold metal transfer welding.

This investigation emphasizes exploring the weldability of ASTM A242 Corten steel using cold metal transfer welding to develop a strong and long-lasting weld that can be used in a wide range of applications including the fabrication of shipping containers, rail wagons, and bridges. However, an effort was made to examine the mechanical and microstructural characteristics of the CMT welded ASTM A242 specimens with crucial variables like welding speed and current and to investigate the potential applications in the fabrication of bridges, railway components, and marine vessels.

2. Experimental Procedure

In the present investigation, ASTM A-242 steel having a thickness of 3 mm, and ER70S-6 filler wire have been used for the CMT welding process. The shielding gas employed in this investigation consists of an 80% Argon-20% Carbon dioxide (CO₂) mixture. This choice is motivated by its capacity to achieve consistent weld penetration, uniform weld bead appearance, and an optimal rate of deposition for the weld metal (Ref 4). For determining the mechanical properties, specimens were prepared with dimensions of 30 × 100 mm, and the sheets were positioned in a butt joint structure. Tables 1 and 2 reveals the chemical composition of the base metal and the filler wire material.

The CMT welding process parameters and their limits used for the experimentation are shown in Table 3. The filler wire selected for this study is copper coated ER70S-6 filler wire of diameter 1.2 mm. The welding input factors were selected using the trial and error experimentation methods performed in the weld bead tests using the Full Factorial method of design matrix to attain the finest outcomes with negligible errors and deep penetration. In this study, weld geometry was visually analyzed by varying the current and welding speed with the uninterrupted flow of shielding gas mixture and torch angle. The cold metal transfer welding setup used for the experimentation purpose is displayed in Fig. 1.

As a part of the pre-welding process, each sample was mechanically cleaned with a stainless steel brush and 99.99% pure acetone was used to take out the foreign materials as well as an oxide deposit present on the material surface. The samples

were also tightly held using welding fixtures to avoid distortion during the welding process.

In order to conduct metallographic investigation, the Corten steel welded specimens were cross-sectioned along the direction of the welding. The metallographic study examines the macrostructure of the weld fusion zone to find weld defects, such as penetration, blowholes, and porosity. Specimens for optical microscopy studies were prepared by various metal finishing processes like surface grinding, polishing along with etching process using the solution of 10 ml of 40% HF, 30 ml of 65% HNO₃, and 20 ml glycerine. The microstructure of three distinct zones identified as parent metal region, fusion zone and heat-affected zone has been examined using a material analysis microscope model Leica DM2500M under multiple combinations of different welding conditions. Furthermore, the fractography of these tensile samples has been examined with a TESCAN Vega 3 Scanning Electron Microscope (SEM). ASTM E8/E8M-16a is the standard used for preparing the tension test sample from the welded specimen. Tensile testing of weld specimens was carried out at room temperature with a loading rate of 1 mm/min to explore the mechanical behavior. The ASTM E190-14 standard was followed in the preparation of the weld models used for the bending test evaluation. The micro hardness of the weld joints was evaluated by determining the penetration level of the indenter into the sample using the Vickers hardness tester under the ASTM E92-17 standard. The hardness test requires a 500 Kgf load with a dwell duration of 10 s. Table 4 depicts the transverse macro-cross-sectional views of welded beads achieved by employing varying welding input factors, including welding speed and current, on ASTM A-242 Corten steel sheets. After analyzing the weld morphology from various levels of process parameters, the optimal process parameters were selected. As part of the ASTM E3-11 standard metallographic method, samples were cleaned and etched with a combination of distilled water, hydrochloric acid (HCl), and nitric acid (HNO₃) before getting ready for macrograph imaging process. Chemical analysis is performed for detecting the base metal's chemical composition, whereas EDAX is used to investigate the weld area. The Welding Expert software was utilized to analyze the optical images, as depicted in Fig. 2, in order to ascertain the dimensions of the weld bead's width and the depth of penetration.

It is evident that there is partial penetration in the weld joint with certain flaws when the current is low and the speed is high (Ref 11). The increase in temperature input causes the depth of penetration to rise, improving the weld's appearance. The difference in size of the top and bottom weld bead decreases as the welding current is increased. As a result, the parent metal melts at greater temperatures and has more time to transmit heat from the CMT joining process into the bottom from the top during the weld pool's solidification. Due to limited heat input, the depth of penetration is slightly unequal between the top and bottom for high speed and low current. Elevated levels of welding current intensity may lead to the creation of thermal

Table 1 Chemical composition of ASTM A-242 corten steel

Grade	C	Mn	Cr	Si	S	Cu	P
ASTMA 242	Max0.12	Max1	0.3-1.25	Max0.75	Max0.03	0.25-0.55	0.06-0.15

Table 2 Chemical and mechanical properties of ER70S6 filler wire

Chemical composition										
Element	C	Si	Mn	P	S	Ni	Cr	Mo	Cu	V
%	0.06	0.81	1.41	0.008	0.011	0.05	0.03	0.01	0.01	0.005

Table 3 CMT welding parameters and levels

Parameters	Units	Levels		
		- 1	0	+ 1
Welding current	A	120	130	140
Welding speed	mm/min	300	325	350

**Fig. 1** Photographic view of cold metal transfer machine

stress, which has the potential to diminish the mechanical characteristics of both the parent material and the CMT welded joint (Ref 12). The symmetrical weld bead geometry produces a linear heat input on the base metal and a constant molten weld pool formation, which leads to a smaller weld bead width and a higher depth of penetration. As a result, it has been determined that combining a lower welding speed with an increased welding current is the most successful technique for obtaining both adequate penetration depth and superior weld quality. As a result, the revised parameters for cold metal transfer welding used in this study to evaluate the mechanical characteristics of Corten steel sheets are 140 A welding current and 300 mm/min welding speed (Joint-3).

3. Results and Discussion

The influence of welding speed and welding current on the weld bead geometry, mechanical properties, microstructure, and fracture surface morphology of CMT welded Corten steel sheets and parent material has been investigated. Initially, a visual checking was carried out to ensure that seams were welded with complete depth of penetration and had been free of weld defects such as porosity and cracks using Welding Expert

software. Tensile and bend tests have been carried out on the CMT Welded sheets using optimized weld parameter settings. To determine the hardness of the weldments, a Vickers hardness test was done. Furthermore, the fractography analysis was observed using a scanning electron microscope.

3.1 Macro- and Microstructure Examination

The various locations of the optical microscope examination of the parent metal region, HAZ and fusion zone are displayed in Fig. 3.

The base metal comprises ferrite and pearlite grains in a heterogeneous distribution (refer to Fig. 4). For better understanding various magnifications such as 50 and 25 μm were viewed and displayed in Fig. 4(a) and (b) and it reveals that ferrite and pearlite structure was viewed.

Figure 5 show the heat-affected zone (HAZ) at 50 μm magnifications of CMT welded ASTM A 242 Corten Steel whereby the microstructure of the parent metal is similar. The thermal impact of weld bead deposition promotes grain size development in the HAZ of the weld joint.

The HAZ exhibits prominent pearlite grains, revealing the impact of heat treatment generated throughout the joining process. In the heat-affected zone formed by the welding heat cycles, there was a complex recrystallized microstructure composed of coarse-grained ferrite, acicular ferrite, tiny discontinuous pearlite colonies, and some grains of bainite along the boundary of the fusion line. The welded joint's fusion zone Fig. 6 displays a microstructure generated by decreased recrystallization, with a pearlitic microstructure and reduced grain boundaries with degenerated pearlite regions. The structure of degenerated pearlite phases was different from the pearlite formed through normalizing and slow cooling treatment (Ref 13). In arc welding process, the cooling rate can be influenced by factors such as the heat input, welding speed, and the material's thermal conductivity. A higher cooling rate implies that the metal is cooling down rapidly after being welded, potentially preventing the formation of pearlite. However, careful examination at 50 μm magnification of fusion zone indicated the presence of numerous coarse pearlites and ferrites structures due to impact of the heat treatment during the welding process.

Figure 7(a) displays the development of a ferrite-pearlite microstructure in the Corten steel base metal. It illustrates that the pearlite is uniformly distributed, which increases the contact area between the pearlite and the ferrite grains. The pearlite phase forms a well-defined network, as seen in Fig. 7(a). As a result due to the preferential dissolution of ferrite, the development of a porous carbide layer can be predicted. Corten steels normally possess a ferrite-pearlite aggregate microstructure, but the addition of alloying elements for strengthening purposes may cause to create a matrix of ferrite that is completely pure with a very fine dispersion of alloy carbides. This reduces the impact of the toughness-reducing

Table 4 CMT welded bead macro cross sections using different welding parameters

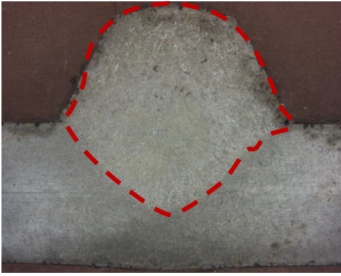



Joint no.	Welding current, A	Welding speed, mm/min	Macroscopic view of sample cross-section
1	120	300	
2	130	300	DoP = 1.9213 Width = 5.4226 
3.	140	300	DoP = 2.3526 Width = 5.7554 
4.	120	325	DoP = 5.3966 Width = 5.7834 
			DoP = 1.7980 Width = 4.7249

Table 4 continued

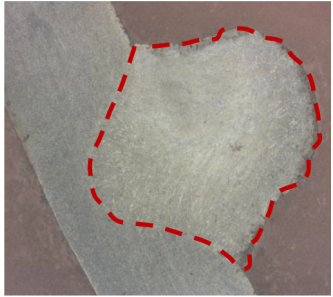


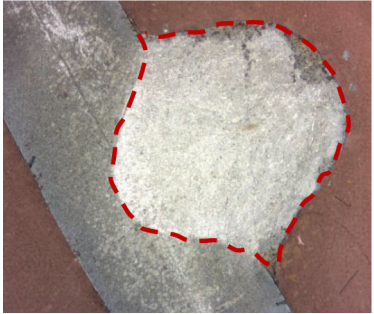
Joint no.	Welding current, A	Welding speed, mm/min	Macroscopic view of sample cross-section
5.	130	325	
6.	140	325	DoP = 2.2730 Width = 5.0649 
7.	120	350	DoP = 4.6196 Width = 5.3085 
8.	130	350	DoP = 1.6450 Width = 5.2522 
			DoP = 1.8788 Width = 5.4138

Table 4 continued

Joint no.	Welding current, A	Welding speed, mm/min	Macroscopic view of sample cross-section
9.	140	350	



DoP = 2.6002 Width = 5.5738

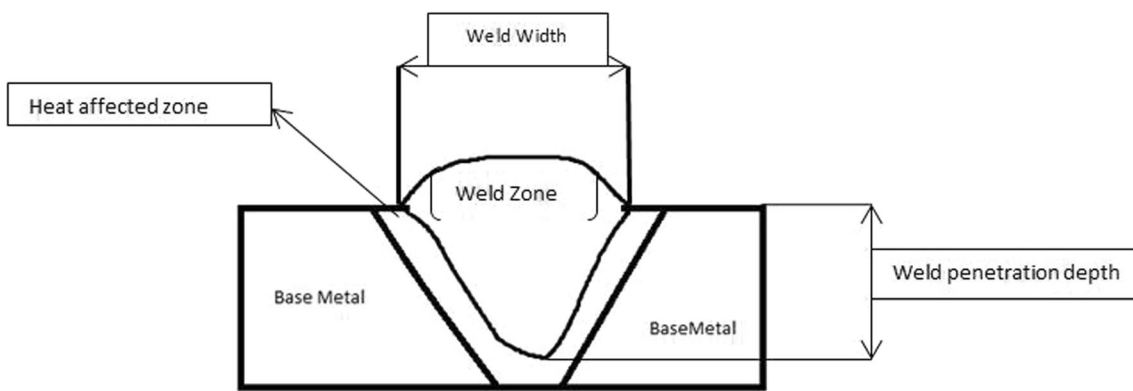


Fig. 2 Weld geometry showing the penetration depth

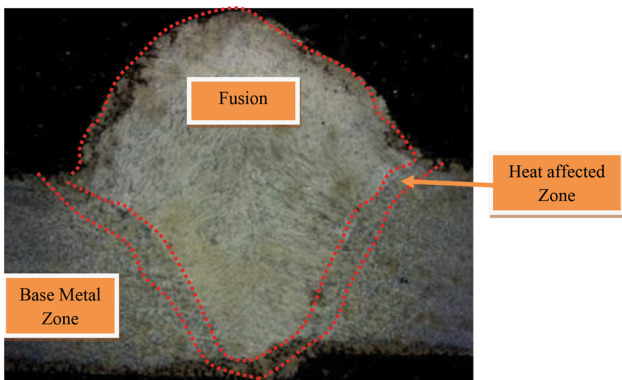


Fig. 3 Weld bead geometry

effect caused by the presence of pearlitic structures, while simultaneously preserving and bolstering the material's strength through the reduction of grain size. From Fig. 7(b) the weld interface which differentiates between the fusion zone and heat-affected zone is visible. The Acicular ferrite-dominated microstructure is visible in the microstructure of the Fusion zone after the CMT welding process. Increased austenitizing temperature induces the formation of acicular ferrite in addition

to the dissolution of pearlite and ferrite. However, more dendrites have been observed in the region of the fusion zone. As a diffusion reduction reaction, acicular ferrite transformation is more likely to occur at the relatively low temperatures of CMT welding because the diffusion rate of atoms decreases with decreasing temperature. The acicular ferrite is formed by the same transformation mechanism in the same temperature range as bainite (Ref 14). The nucleation of acicular ferrite within austenitic grains demands more energy compared to the nucleation of bainite, which occurs initially at the outermost boundaries of previously generated austenite grains (Ref 15).

3.2 EDAX Analysis

EDAX point investigation was also carried out at the weld zone and is shown in Fig. 8. Higher austenitization temperatures in the weld zone area led to increased dissolution of carbide-forming elements like Nb, V, and Ti, along with greater uniformity in the austenite phase, as confirmed by EDAX examination.

Corten steel welded with a shielding gas mixture of 80% argon and 20% CO₂ indicates the presence of iron, carbon, chromium, silicon, manganese, phosphorus, sulfur, nickel, copper, and vanadium. It was observed that the weld zone of CMT welded ASTM A-242 steel had the presence of enriched

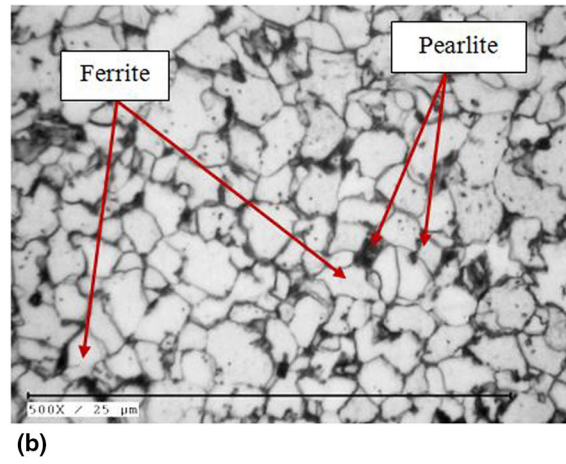
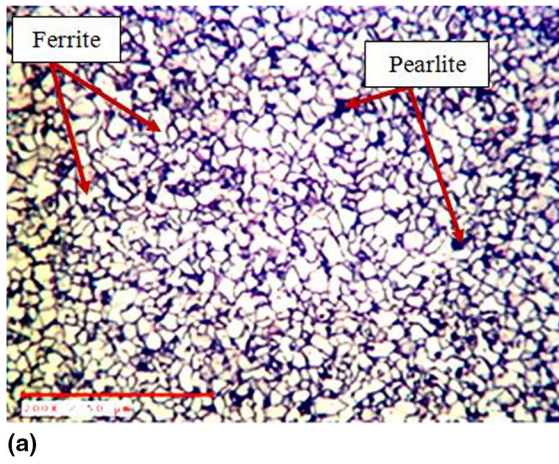


Fig. 4 Microstructures of ASTM A 242 Corten steel (base metal)

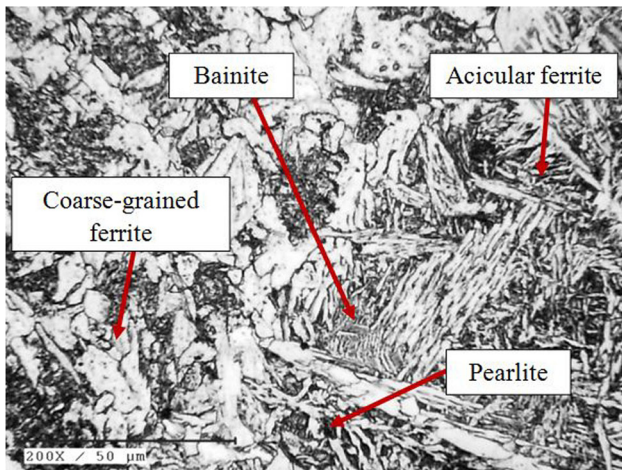


Fig. 5 Microstructures of HAZ of CMT welded ASTM A 242 Corten steel

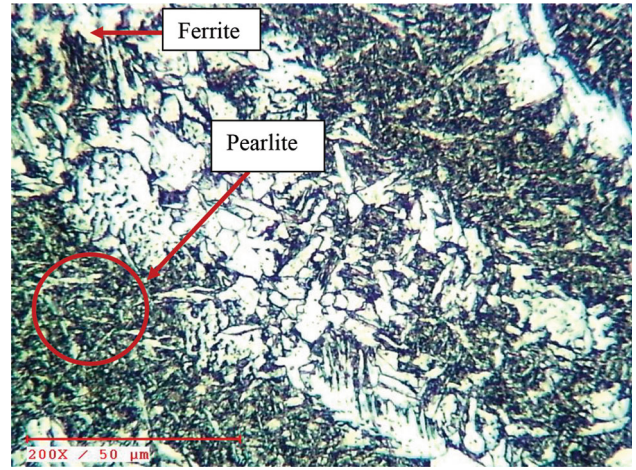


Fig. 6 Microstructures of fusion zone [FZ] of CMT welded ASTM A 242 Corten steel

Fe and C, Cr, and Mn. The presence of chromium in the base material results in corrosion resistance which helps in marine applications. The addition of manganese influences the mechanical properties of Corten steel in the fusion zone (FZ) with the extent of this influence determined by the carbon content. Manganese increases steel's hardenability by reducing the cooling rate during hardening. From the EDAX analysis, it can be seen that the presence of higher amounts of manganese compared to less nickel in the weld zone reveals an improvement in the structure as well as the properties of the material.

3.3 Mechanical Behavior of the Weldments

Figure 9 depicts the test results and variations in micro-hardness from the base metal to the center of the fusion zone. The hardness values were determined by measuring from the center of the fusion zone to the base metal with an equal distance of approximately 1 mm as indicated in Table 5. According to the hardness reports, the highest hardness produced within the weld fusion region of the CMT welded specimen is 270.2 HV.

The area which lies between the weld fusion zone and the coarse-grained heat-affected zone (CGHAZ) exhibits the highest temperature gradient, increasing micro-hardness. This is

simply because the top of the weld bead surface begins to cool quicker than the middle of the weld metal. The occurrence of acicular ferrite and partially unfused grain particles is responsible for the high hardness in the fusion boundary area at all welded joints. Acicular ferrite and unmelted grains appear at the fusion boundaries during the solidification process and are partially used as nuclei by the new precipitating phase of the weld metal.

After reaching this maximum value, the micro-hardness in the temperature-affected region of the welded metal starts to decrease. The micro-hardness similarity of all welded joints within the heat-affected zone is due to a very slow cooling speed in the region adjacent to the weld fusion area. The tensile properties such as ultimate tensile strength and elongation ratio of the weld samples were evaluated. The graphical plots of engineering stress versus engineering strain obtained from the tested samples of base metal and weld metal are clearly shown in Fig. 10 and 11.

The tensile and yield strengths of the base metal are 523.81 and 405.63 MPa, respectively. Similarly, the tensile strength and yield strength of Corten steel sheets welded using the cold metal transfer method are 589.79 and 405.63 MPa, respectively. In comparison, the base metal has a percentage

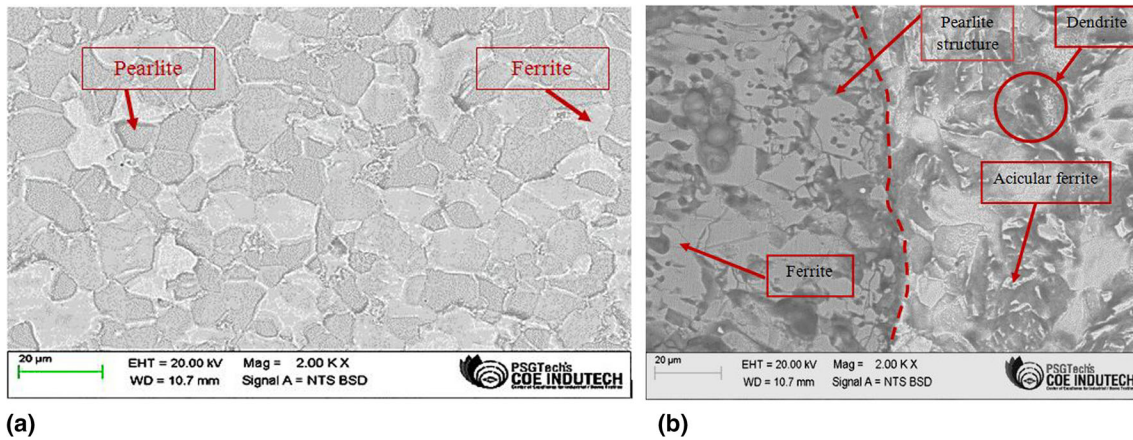


Fig. 7 (a) Scanning electron microscope photographs of (a) ASTM A 242 corten steel (b) CMT welded ASTM A 242 corten steel

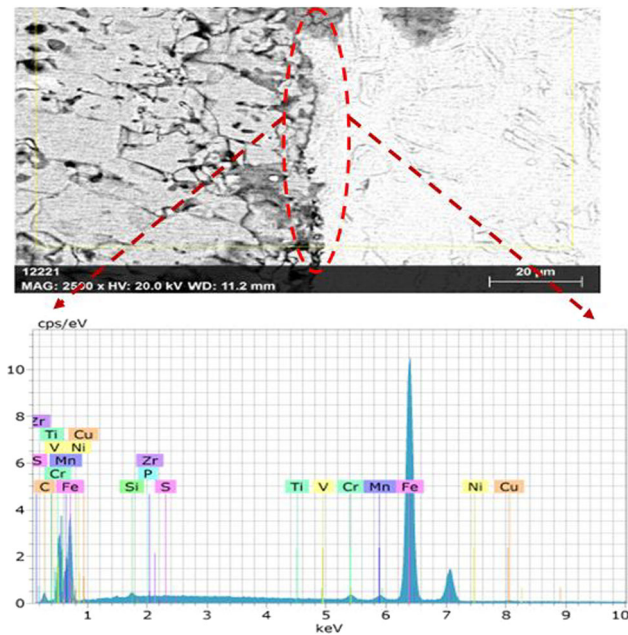


Fig. 8 EDAX Analysis of CMT Welded ASTM A242 corten steel

elongation of 25.95%, whereas the weld metal has an elongation of 16.87%.

Figure 12(a) and (b) indicates the photographs of tensile-tested specimens of ASTM A 242 Corten Steel and CMT welded ASTM A 242 Corten Steel. From Fig. 12(b), it is clear that the fracture has not occurred in the welded region, and the above results confirm that the weld metal is relatively strong and the alloying properties control the chemical composition and microstructure of the welded joint and provide excellent strain hardening in the weldment. Strong carbide/nitride-producing elements such as Ti, V, etc., have extremely limited solubility in ferrite and austenitic, and the precipitate generally behaves as a thin dispersion of carbides and nitrides, contributing to strength as a result of precipitation hardening (Ref 16). This phenomenon arises because the yield strength of all welded joints is increased in comparison to the yield strength of the underlying metal. The interplay between solute atoms and mobile dislocations is accountable for the extension of the yield strength.

The stress–strain curves for the bend test of the face bend-tested specimen and the root bend-tested specimen are illustrated in Fig. 13(a) and (b), indicating that the stress and strain are exactly proportional to each other. Bending tests for ductility provide a quick and easy approach to assessing a material’s quality by its resistance to fractures or other surface defects under continuous bending conditions. In the case of root and face, the face bend possessed a higher yield than the root bend. This was happening because during experimentation, higher loads were acting on the face bend and the counterpart is resisting the load. However, the load was transmitted from the face bend to the root bend at a time extent. Hence the stress was dissipated on the metal surface. It clearly visualizes the root bend region. After three-point bend testing, no cracks or holes were found in the cross-section of the tested specimen. From 13(a) and Fig. 13(b), it was detected that the flexural strength of the sample that is bent with the face outward [797 MPa] is higher than the sample bent with the root side of the weld outward [708 MPa].

Figure 14 shows the stress–strain bending plots of ASTM A242 Steel (Base metal). By comparing Fig. 13(a) and (b) and 14, there is a noteworthy improvement in the bending strength of the CMT welded specimen from the parent metal. The bend tests revealed that the welded joint’s ductility was satisfactory.

3.4 Fracture Analysis

The fractured surfaces of the base metal and CMT welded specimens are shown in Fig. 15 and 16.

During the transverse tensile testing process, all welds fail in the weakest region of base metal. The tensile strength values of the parent metal and the weld metal are 523.81 and 589.79 MPa. It is clear from the tensile micrographs (Fig. 15 and 16) that both welds suffer from severe plastic deformation and exhibit improved strength. As shown in Fig. 15 and 16, deep circular dimples are found on the fractured surface region of the parent metal and the weld metal that undergoes a tensile test. The fractography of the base metal looks very similar to that of the weld metal, but the dimples appear smaller. This was happening because the stress triaxiality of the tensile specimen is smaller. The nucleation of acicular ferrite (Fig. 7b) enhances deformation resistance during tensile testing. Furthermore, air cooling increases the thickness and diameter of the acicular ferrite, raising the material’s tensile strength. Meanwhile, plastic deformation and necking, which are characteristic of

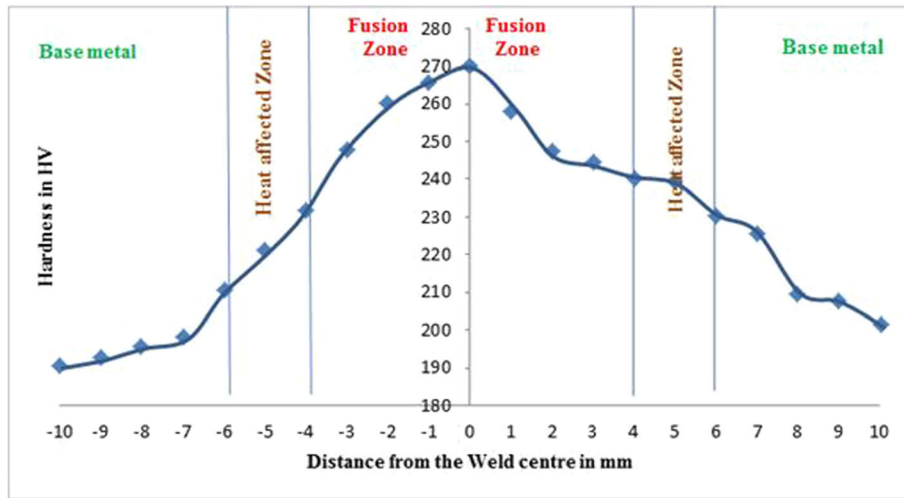


Fig. 9 Vicker's micro-hardness of ASTM A242 Steel CMT welded specimen

Table 5 Vicker's micro-hardness values of ASTM A242 steel CMT welded specimen

Distance from the weld center in mm	Hardness in HV
- 1	265.7
- 2	260.2
- 3	248.1
- 4	231.8
- 5	221.3
- 6	210.9
- 7	198.3
- 8	195.9
- 9	192.8
- 10	190.5
0	270.2
1	258.1
2	247.5
3	244.6
4	240.2
5	239.4
6	230.5
7	225.4
8	209.6
9	207.8
10	201.6

flexural fracture, can be identified in fractured specimens. Dimples and micro-voids, significant elements of ductile fracture, have been clearly visible in all samples, as demonstrated in Fig. 15 and 16.

The fractography of the bend specimen displayed in Fig. 17 reveals the presence of microscopic voids with typical dimples in the area of fracture surfaces. Localized stress concentrations generated micro-voids to emerge as the strain evolved in the plastic deformation zone and at the tip of the crack deformation. The SEM fractography of bended specimen indicates the presence of large and deep-like structures on the fracture

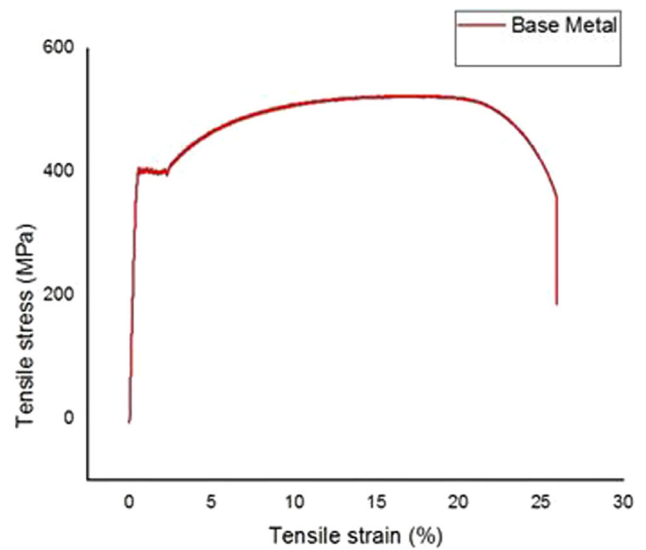


Fig. 10 Plots of tensile stress vs. tensile strain of base metal

surface and some cracked second-phase particles are found at the bottom of the dimple, indicating a typical micro-aggregation fracture mechanism. Some cleavage facets were also observed in the fracture surface which us indicated by blue arrows in Fig. 17. In contrast, the surface characteristics of the fractured weld specimen can vary greatly depending on the applied welding speed.

4. Conclusion

The main objective of this research is to demonstrate the successful joining of ASTM A242 weld joints by applying the cold metal transfer welding method. The following are the conclusions of the current investigation.

- CMT Welded joints created using increased current and reduced speed exhibit optimal weld shape, accompanied by outstanding penetration depth and the absence of weld-

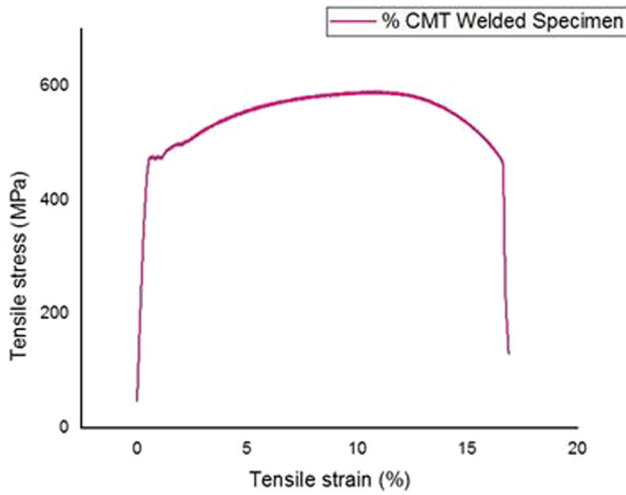


Fig. 11 Plots of tensile stress vs. tensile strain of weld metal

ing defects. The optimized welding parameters selected to study the mechanical characteristics of Corten steel sheets are 140 A welding current and 300 mm/min welding speed.

- The inclusion of pearlite and ferrite in the solidified weld metal refines its grain structure, leading to enhanced

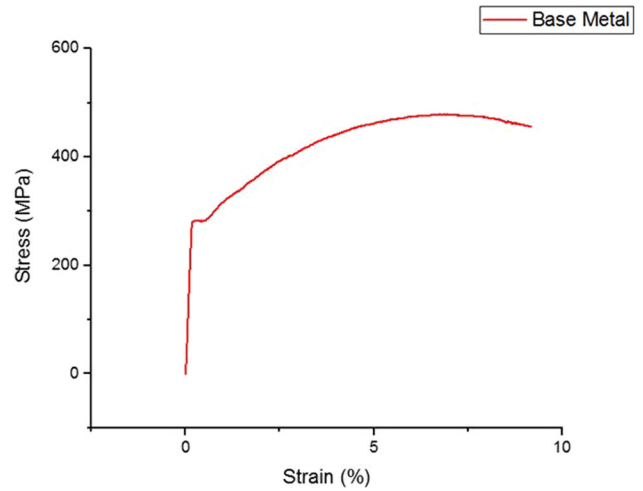


Fig. 14 Stress-strain curve of ASTM A242 steel (base metal)

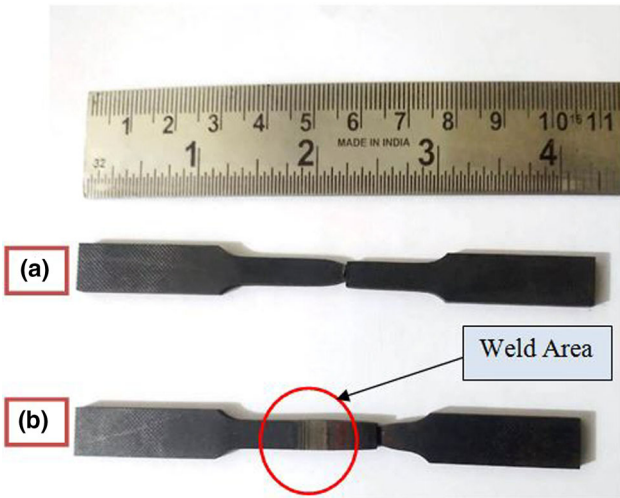


Fig. 12 Tensile-tested specimen (a) ASTM A 242 corten steel (b) CMT welded ASTM A 242 corten steel

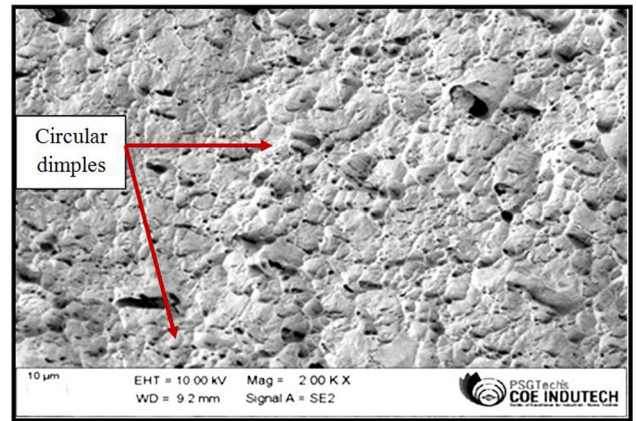


Fig. 15 SEM fractography of base metal

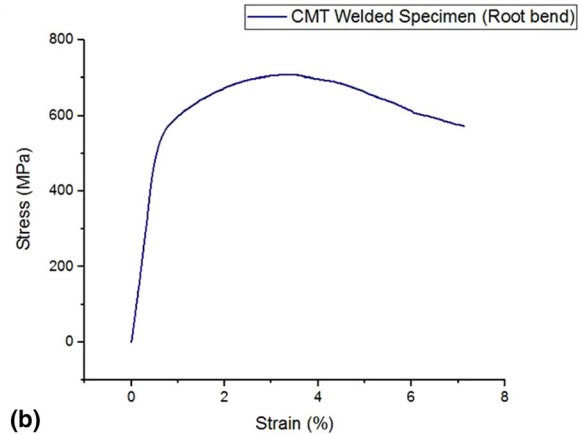
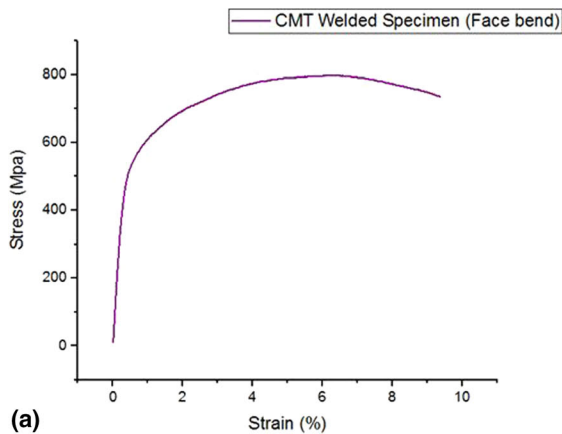


Fig. 13 (a) Stress-strain curve of CMT welded specimen (Face bend) (b) stress-strain curve of CMT welded specimen (Root bend)

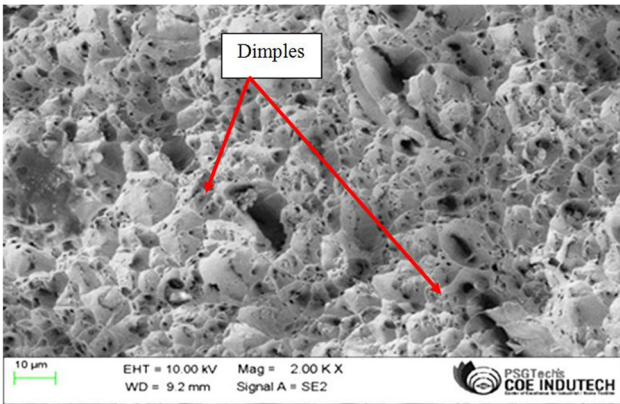


Fig. 16 SEM fractography of weld metal

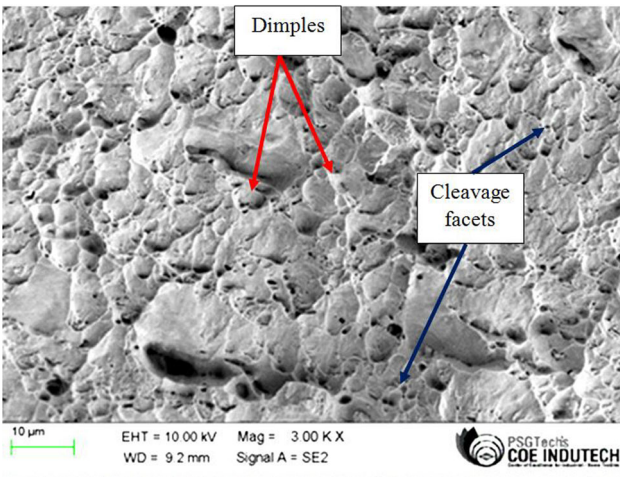


Fig. 17 SEM fractography of bended specimen

mechanical properties and increased resistance to cracking.

- Tensile test reveals that the base metal exhibits a percentage elongation of 25.95%, while the weld metal has an elongation of 16.87%.
- The maximum Vicker's hardness acquired is 270.2 HV located in the weld fusion region of the CMT welded specimen when compared with the base metal zone and heat-affected zone.
- The fracture micromorphology in base metal reveals the appearance of smaller dimples as well as a minimal number of large dimples due to the low-stress triaxiality of the tensile specimen.
- Bending test illustrated that the flexural strength of the sample bent with the face outward [797 MPa] is greater than the flexural strength of the sample bent with the root side of the weld outward [708 MPa].
- Bending test weld specimen fracture surfaces demonstrate the existence of micro-voids, cleavage facets with general dimple formations because of the plastic deformation zone and stress at the crack tip.

This research focuses on the possibilities of using Corten steel sheet for the manufacture of rail coaches, bridges, roof walls of

buildings, and shipping containers due to its excellent weldability and excellent mechanical properties.

Funding

The author(s) indicated that there is no funding associated with the work described in this article.

Conflict of interest

The author(s) declared no potential conflicts of interest.

References

1. M.S. Reddy, G.V.S. Kumar, T. Bhaskar, and K. Sivaprasad, Mechanical Behaviour, Microstructure and Texture Studies of Wire Arc Additive Manufactured Corten Steels, *Trans. Indian Inst. Met.*, 2023, **76**(2), p 519–526. <https://doi.org/10.1007/s12666-022-02725-z>
2. D. Kumaravel and V.K. Bupesh Raja, Effect of Recrystallization Temperature on Metallurgical Properties of ASTM A242 Corten Steel, *Key Eng. Mater.*, 2022, **933**, p 124–128. <https://doi.org/10.4028/p-61m1v8>
3. V. Vairamani, N. Mohan, S.K. Karthikeyan, and M. Sakthivel, Optimization and Microstructure Analysis of Corten Steel Joint in Mag Welding by Post Heat Treatment, *Mater. Today*, 2020, **21**, p 673–680. <https://doi.org/10.1016/j.matpr.2019.06.737>
4. B. John, S. Paulraj, and J. Mathew, The Role of Shielding Gas on Mechanical, Metallurgical and Corrosion Properties of Corten Steel Welded Joints of Railway Coaches Using Gmaw, *Adv. Sci. Technol. Res. J.*, 2016, **10**(32), p 156–168. <https://doi.org/10.12913/22998624/65119>
5. R.F. Assumpção, A.P. Silva, V.F.C. Lins, and D.C. Sicupira, Corrosion Performance of New-Type Si-Based Weathering Steel in Marine Environment, *J. Mater. Eng. Perform.*, 2022 <https://doi.org/10.1007/s11665-022-07737-w>
6. S. Selvi, A. Vishvakshenan, and E. Rajasekar, Cold Metal Transfer (CMT) Technology—An Overview, *Def. Technol.*, 2018, **14**(1), p 28–44. <https://doi.org/10.1016/j.dt.2017.08.002>
7. S.K. Gupta, A.P. Patil, R.C. Rathod, V. Tandon, and H. Vashishtha, Tailoring the Process Parameters for Ti-Stabilized 439 Ferritic Stainless Steel Welds by Cold Metal Transfer Process, *J. Mater. Eng. Perform.*, 2023, **32**(13), p 6042–6053. <https://doi.org/10.1007/s11665-022-07534-5>
8. H. Shanker and R. Wattal, A Comprehensive Survey on the Cold Metal Transfer Process in Welding Similar and Dissimilar Materials and for Cladding, *Proc. Inst. Mech. Eng. Part C*, 2022, **237**(10), p 2360–2391. <https://doi.org/10.1177/09544062221139947>
9. P. Kah, R. Suoranta, and J. Martikainen, Advanced Gas Metal Arc Welding Processes, *Int. J. Adv. Manuf. Technol.*, 2012, **67**(1–4), p 655–674. <https://doi.org/10.1007/s00170-012-4513-5>
10. T. Guo, Z. Dong, X. Nan, X. Liu, and L. Zhang, Effect of Welding Material on Microstructure and Properties of Welded Joints of Bridge Weathering Steel Q345qDNH, *Materialwiss. Werkstofftech.*, 2022, **53**(11), p 1334–1346. <https://doi.org/10.1002/mawe.202200070>
11. A.R. Kannan, N.S. Shanmugam, and S.A. Vendan, Effect of Cold Metal Transfer Process Parameters on Microstructural Evolution and Mechanical Properties of AISI 316L Tailor Welded Blanks, *Int. J. Adv. Manuf. Technol.*, 2019, **103**(9–12), p 4265–4282. <https://doi.org/10.1007/s00170-019-03856-2>
12. K. Schmidt, J.P. Bergmann, E. Spaniol, M. Trautmann, and U. Füssel, The GMAW Process Using a Two-Dimensional Arc Deflection with AC Hot Wires, *Weld. J.*, 2023, **102**(4), p 88–96. <https://doi.org/10.29391/2023.102.007>
13. G.T. Park, S.U. Koh, H.G. Jung, and K.Y. Kim, Effect of Microstructure on the Hydrogen Trapping Efficiency and Hydrogen Induced Cracking of Line Pipe Steel, *Corros. Sci.*, 2008, **50**(7), p 1865–1871. <https://doi.org/10.1016/j.corsci.2008.03.007>

14. S.S. Babu and H.K.D.H. Bhadeshia, Mechanism of the Transition from Bainite to Acicular Ferrite, *Mater. Trans. JIM*, 1991, **32**(8), p 679–688. <https://doi.org/10.2320/matertrans1989.32.679>
15. S.S. Babu and H.K.D.H. Bhadeshia, Transition from Bainite to Acicular Ferrite in Reheated Fe-Cr-C Weld Deposits, *Mater. Sci. Technol.*, 1990, **6**(10), p 1005–1020. <https://doi.org/10.1179/026708390790189605>
16. I. Brown, The Role of Micro segregation in Centreline Cold Cracking of High Strength Low Alloy Steel Weldments, *Scr. Mater.*, 2006, **54**(3), p 489–492. <https://doi.org/10.1016/j.scriptamat.2005.09.047>

Publisher's Note Springer Nature remains neutral with regard to jurisdictional claims in published maps and institutional affiliations.

Springer Nature or its licensor (e.g. a society or other partner) holds exclusive rights to this article under a publishing agreement with the author(s) or other rightsholder(s); author self-archiving of the accepted manuscript version of this article is solely governed by the terms of such publishing agreement and applicable law.